Photo-excited in situ loading of Pt clusters onto rGO immobilized SnO_2 with excellent catalytic performance toward methanol oxidation

Shouliang Wu [a], Jun Liu [a], Dewei Liang [a, b], Hongmei Sun [a, b], Yixing Ye [a], Zhenfei Tian[a] and Changhao Liang [a, b*]

[a] *Key Laboratory of Materials Physics and Anhui Key Laboratory of Nanomaterials and Nanotechnology, Institute of Solid State Physics, Chinese Academy of Sciences, Hefei 230031, China.*

[b] *Hefei National Laboratory for Physical Sciences at the Microscale, University of Science and Technology of China, Hefei, 230026, China*

*Corresponding author. Tel: +86 55165591129; Fax: Tel: +86 55165591434;

E-mail: chliang@issp.ac.cn (C.H. Liang)

Abstract

Great effort is made to maximize the surface area and expose active sites of a catalyst by distributing it over a suitable electronic conducting support. We present a design and eco-friendly construction of a two-dimensional Pt/SnO_2/reduced-graphene-oxide (rGO) nanocomposite to study the strong metal-semiconductor-support interactions as candidate highly active and durable electrocatalyst. Distinctively, highly reactive SnO_x nanoparticles (NPs) induced by laser ablation in liquids were used as a precursor to transform the graphene oxide (GO). Simultaneously, the initial amorphous-like SnO_x further crystallized into SnO_2 NPs, which were uniformly anchored onto rGO sheets. Afterward, the photo-excited electrons from semiconductor SnO_2 were used as green reducing agents. Ultrafine Pt NPs with an average size of about 1–2 nm were *in situ* reduced and uniformly anchored on the surface of crystallized SnO_2 NPs. Compared with the Pt/rGO catalysts without SnO_2 modification, the prepared Pt/SnO_2/rGO catalysts not only show larger electrochemical active surface area and higher catalytic activity toward methanol oxidation but also exhibit better tolerance toward CO and long-term cycle stability. The significantly enhanced electrochemical performance should be attributed to the uniformly dispersed Pt NPs with ultrafine size and the synergetic effect from the hybrid noble metal-semiconductor-carbon network components, which possess promising potential applications as electrocatalysts for methanol oxidation.

KEYWORDS: Pt cluster; hybrid composite electrocatalyst; photo-excited reduction; methanol oxidation; laser ablation in liquids

Abstract

Great efforts have been made to maximize the surface area and expose active sites of catalysts by distributing them over a suitable electronic conducting support.

Maximizing the surface area and exposing the active sites of Pt-based catalysts is one of the most effective strategies to improve their electrocatalytic properties.

Here, we present an eco-friendly design in constructing two-dimensional Pt/SnO_2/reduced-graphene-oxide (rGO) nanocomposites (NCs). Firstly, SnO_2 nanoparticles (NPs) uniformly decorated rGO sheets (SnO_2/rGO NCs) were prepared by a reductive reaction between graphene oxide (GO) and highly reactive SnO_x NPs induced by laser ablation in liquids. Afterward, by using the photo-excited electrons from SnO_2/rGO as green reducing agents, ultrafine Pt NPs with an average size of about 1–2 nm were *in situ* anchored on the surface of SnO_2 NPs. These obtained Pt/SnO_2/rGO NCs were used as electrocatalysts for methanol oxidation, compared with the Pt/rGO catalysts, which not only present higher catalytic activity, but also exhibit better tolerance toward CO-like species and long-term cycle stability. The significantly enhanced electrochemical performance should be attributed to the uniformly dispersed Pt NPs with ultrafine size-distribution and the synergetic effect derived from the noble metal-semiconductor-carbon network hybrid components. These findings suggest that such Pt/SnO_2/rGO NCs possess promising potential applications as electrocatalysts for methanol oxidation.

KEYWORDS: Pt cluster; hybrid composite electrocatalyst; photo-excited reduction; methanol oxidation; laser ablation in liquids

Introduction

Fuel cells, especially direct methanol fuel cells (DMFCs), have attracted considerable attention because of environmental problems caused by the consumption of fossil fuels and the urgent demands for clean energy systems [1, 2]. DMFCs can be operated at a low temperature and possess high energy conversion efficiency. Hence, DMFCs are promising as new power sources for mobile and portable electronic devices [3−5]. However, the successful commercialization of DMFCs was greatly hampered by the high manufacturing cost, slow reaction kinetics of Pt-based catalysts, and the poisoning of Pt catalysts by CO-like species during the process of methanol oxidation [6, 7].

For application in methanol oxidation, Pt catalysts with ultrafine sizes are highly desirable because of their increased surface area and large amounts of corner and edge atoms. Thus, downsizing the Pt NPs is not only beneficial for improving the catalytic activity but can also reduce the usage amount and manufacturing cost of the Pt catalysts. Nevertheless, owing to their high surface energy, ultrafine Pt NPs have a tendency to aggregate into larger species under reaction condition, which would cause a serious decline in their performance for methanol oxidation. One of the effective strategies for solving these deactivation problems involves uniformly loading the catalysts on a suitable supporting material that has a low cost, high surface area, and excellent conductivity. As a two-dimensional carbon material with single atomic layer, graphene has recently attracted increased attention due to its potential application as excellent catalyst supporting material in fuel cells [8−12]. It possesses a large specific

surface area to provide efficient catalyst particle dispersion, a high electrical conductivity to facilitate the fast electron transfer, a superior thermal and chemical stability to avoid corrosion, and a dense honeycomb crystal structure to promote gas flow.

In addition, to improve the CO poisoning tolerance of Pt catalysts, one of the widely accepted methods is to directly add metal oxides (TiO_2, SnO_2, SiO_2, and CeO_2) as additives for Pt catalysts [13−16]. Firstly, the low price and abundance of metal oxides are beneficial to reduce the manufacturing cost of catalysts. At the same time, the use of metal oxides can effectively promote the uniform dispersion of Pt NPs, thereby favoring the increase of active surface per weight of Pt. More importantly, most of the metal oxides possess a great capacity for storing and releasing oxygen, which would play an important role in further oxidizing the CO-like species. However, metal oxides possess poor electron conductivity, which makes it difficult to achieve sufficient electrocatalytic properties by integrating with Pt catalysts.

Therefore, to combine the excellent features of metal oxides and outstanding electronic conductivity as well as large surface area of graphene, kinds of Pt/metal-oxides/rGO NCs have been synthesized and investigated as electrocatalysts for methanol oxidation [17-20]. For example, Wang and his co-workers have prepared Pt/TiO_2/rGO catalysts with significantly enhanced catalytic activity and stability toward methanol oxidation [17]. The Pt/CeO_2/rGO catalysts prepared by Geng's group showed lower over-potential, much higher catalytic activity, and stability for methanol oxidation compared with that of the Pt/rGO catalysts [18]. However, it

should be noted that most of their synthetic methods either used sodium borohydride or hydrazine hydrate as the reducing agents, which are highly toxic and may cause serious environmental or health problems, thereby limiting their practical uses in a general case. In addition, surfactants such as poly-vinylpyrrolidone (PVP) are usually introduced as stabilizers to control the particle growth. These stabilizers could be strongly absorbed on the surface of Pt catalysts and then severely affect their catalytic performance. More importantly, a large proportion of Pt precursor would associate with graphene rather than metal oxides because of the higher surface area and adsorbability of graphene. Thus, many reduced Pt catalysts disperse only on the surface of graphene and cannot effectively attach onto the metal oxides.

We propose a simple and green strategy to fabricate a two-dimensional Pt/SnO_2/rGO hybrid nanocomposite (NC) based on laser ablation in liquids (LAL) technique combined with a facile photo-assisted *in situ* reduction method. Several benefits of this work are inspired, as follows: (i) the photo-excited electrons from SnO_2 NPs were used as clean reducing agents and no organic surfactant was introduced during the whole synthetic process; (ii) the reduction reaction of Pt occurred on the surface of SnO_2, thereby leading to the ultrafine Pt NPs *in situ* anchoring on the surface of SnO_2 NPs; (iii) this synthetic method has successfully produced ultrafine Pt NPs with an average size of about 1–2 nm, which were evenly distributed on the surface of SnO_2; and (iv) the as-prepared Pt/SnO_2/rGO catalysts present higher catalytic activity and better long-term performance toward methanol oxidation compared with the Pt/rGO catalysts.

Experimental

2.1 Chemical reagents and materials

All reagents used in the present experiments were of analytical grade and applied without further purification. Graphite powder was purchased from Tianjin Guangfu Fine Chemical Research Institute. GO was synthesized from graphite by using a modified Hummers method [21, 22]. Double-distilled water (resistance, >18 MΩ cm^{-1}) was used throughout all experiments.

2.2 LAL-assisted preparation of SnO_2/rGO NCs

The highly dispersed SnO_2 NPs decorated rGO sheets were first prepared according to our previous report [23]. Briefly, by fixing the polished tin plate (99.99% in purity) in a vessel filled with 15 mL deionized water, the rotating metal plate will be ablated for 5 min by a fundamental Nd:YAG laser (1064 nm) with 10 Hz pulse repetition rate, 10 ns pulse duration, and 80 mJ per pulse laser energy. After ablation, the obtained fresh colloidal solution was quickly mixed with 2 mL GO solution (8×10^{-5} g/mL) and was placed inside a dark chamber. A week later, the newly prepared SnO_2/rGO NCs were collected by centrifugation.

2.3 Photo-assisted in situ reduction route for Pt/ SnO_2/rGO NCs

The ultrafine Pt NPs were *in situ* reduced under UV-light irradiation. Prior to irradiation, the above-obtained SnO_2/rGO precipitates and 2 mL chloroplatinic acid (H_2PtCl_6, 4 mg/mL) were added into a 50 mL test tube containing 30 mL deionized water. After ultrasonic treatment for 10 min, the mixture was illuminated by a 300 W mercury lamp at room temperature for 90 min with a distance of 40 cm. The black

precipitates were collected by centrifugation and washed with deionized water for three times. The final products were obtained by drying the precipitates at 50 °C in a vacuum-drying box. By adjusting the amounts of added H_2PtCl_6 solution (1, 2, and 3.5 mL) without changing any other parameters, a series of catalysts with different mass ratios of Pt and SnO_2 can be obtained and denoted as $Pt_{0.77}/SnO_2$/rGO, $Pt_{0.89}/SnO_2$/rGO, and $Pt_{1.21}/SnO_2$/rGO, respectively. The mass ratio of Pt and SnO_2 in different prepared catalysts was determined by inductively coupled plasma atomic emission spectroscopy (ICP-AES) tests.

2.4 Preparation of Pt/rGO NCs

For comparison, Pt/rGO NCs were synthesized by a chemical method modified from other reports [24, 25]. In a typical synthesis, 0.6 mL H_2PtCl_6 solution (4 mg/mL) and 0.2 mL HCOOH were added to 15 mL GO solution (8×10^{-5} g/mL). After ultrasonic treatment for 30 min, the suspension was stored at room temperature for 48 h. Finally, the precipitates were washed with deionized water for three times and dried at 50 °C in a vacuum-drying box.

2.5 Structure characterization

The surface chemical constituents of the prepared catalysts were analyzed by X-ray photoelectron spectroscopy (XPS, Thermo ESCACLB 250). Transmission electron microscopy (TEM) images were captured on a JEOL-2010 apparatus with 200 kV accelerating voltage. High-angle annular dark-field scanning transmission electron microscopy (HAADF-STEM) images were recorded on a JEM-ARM-200F instrument (University of Science and Technology of China). Before TEM

examination, the products were ultrasonically dispersed in ethanol and then a drop of the suspension was deposited onto a Cu grid coated with a thin carbon film.

2.6 Electrochemical measurements

All electrochemical measurements were performed in a standard three-electrode Zahner IM6e electrochemical workstation. A Pt wire and a KCl-saturated Ag/AgCl electrode were used as the counter and reference electrodes, respectively. A glassy carbon (GC) electrode (3 mm in diameter) was polished to a mirror finish with Al_2O_3 slurry (0.3 μm) and ultrasonically cleaned in ethanol for a few minutes. Subsequently, 10 μL of the as-prepared catalyst suspension was directly pipetted onto the working electrode, followed by solvent evaporation at room temperature. Exactly, 20 μL of Nafion solution was then dropped onto the dried sample. The weight of Pt on each working electrode was calculated through ICP measurement. 0.5 M N_2-saturated H_2SO_4 aqueous solution was used as electrolyte for measuring the electrochemical active surface area (ECSA) of the catalysts. The cyclic voltammetry (CV) measurements for evaluating the methanol oxidation performance were performed at a scan rate of 50 mV s^{-1} in a mixed solution consisting of 0.5 M H_2SO_4 and 0.5 M CH_3OH. The current time (CA) curves were recorded at a constant potential of 0.615 V for 60 min in a solution of 0.5 M H_2SO_4 containing 0.5 M CH_3OH. To further assess the stability of each catalyst, long-term CV tests (1200 cycles) were conducted within a potential range of 0 to 1 V at a scan rate of 50 mV s^{-1}.

Results and Discussion

3.1 Strategy for synthesizing Pt/SnO_2/rGO NCs

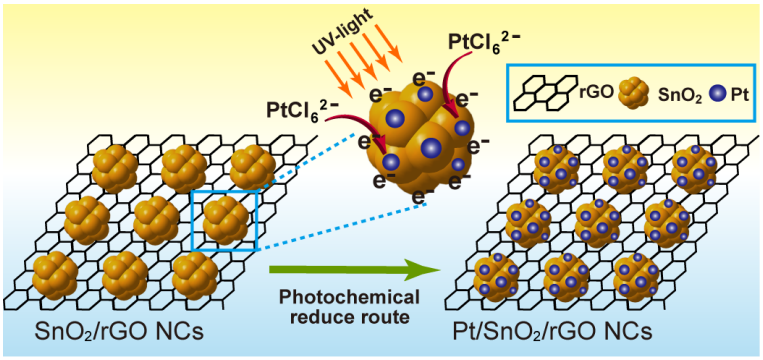

Scheme 1. Illustration for the synthesis of Pt/SnO_2/rGO NCs.

We proposed the formation mechanism of Pt/SnO_2/rGO NCs in our synthesis strategy as follows. In our previous reports, we have repeatedly proved that most fresh colloids generated by LAL technique possess high activity and reactivity [26−28]. In the present effort, LAL-induced fresh SnO_x colloids showing a low valence state of cation Sn and poor crystallization were first dispersed on the surface of GO sheets. After aging treatment at room temperature, GO sheets *in situ* evolved into rGO sheets, whereas the poorly crystalline SnO_x NPs were simultaneously converted into well-crystallized SnO_2 NPs and uniformly distributed on rGO sheets as well, as shown in Figure S1. Expectedly, the high distribution of SnO_2 NPs on rGO sheets would result in high dispersion of Pt catalysts. Scheme 1 shows the synthesis process of the Pt/SnO_2/rGO NCs. Under the UV-light irradiation, the photo-excited electrons migrated from the valence band of SnO_2 NPs to the conduction band, leaving the holes in the valence band. The $PtCl_6^{2-}$ absorbed on the surface of SnO_2 was then *in situ* reduced to Pt^0 atom by the photo-excited electrons. Then, many reduced Pt atoms aggregated into ultrafine Pt NPs, which were uniformly anchored on the surface of SnO_2. The mechanism of this reduction reaction can be expressed in the following

formulas:

(a) adsorption of $PtCl_6^{2-}$ on the surface of SnO_2

$$PtCl_6^{2-} + SnO_2 \leftrightarrow SnO_2\text{-}(PtCl_6^{2-})_{ads} \quad (1)$$

(b) creation of electron-hole pairs

$$SnO_2 + h\nu \rightarrow e^- + h^+ \quad (2)$$

(c) reduction of ultrafine Pt NPs

$$SnO_2\text{-}(PtCl_6^{2-})_{ads} + ne^- \rightarrow SnO_2\text{-}Pt_{(NPs)} + Cl^- \quad (3)$$

3.2 Characterization of the prepared Pt/SnO₂/rGO NCs

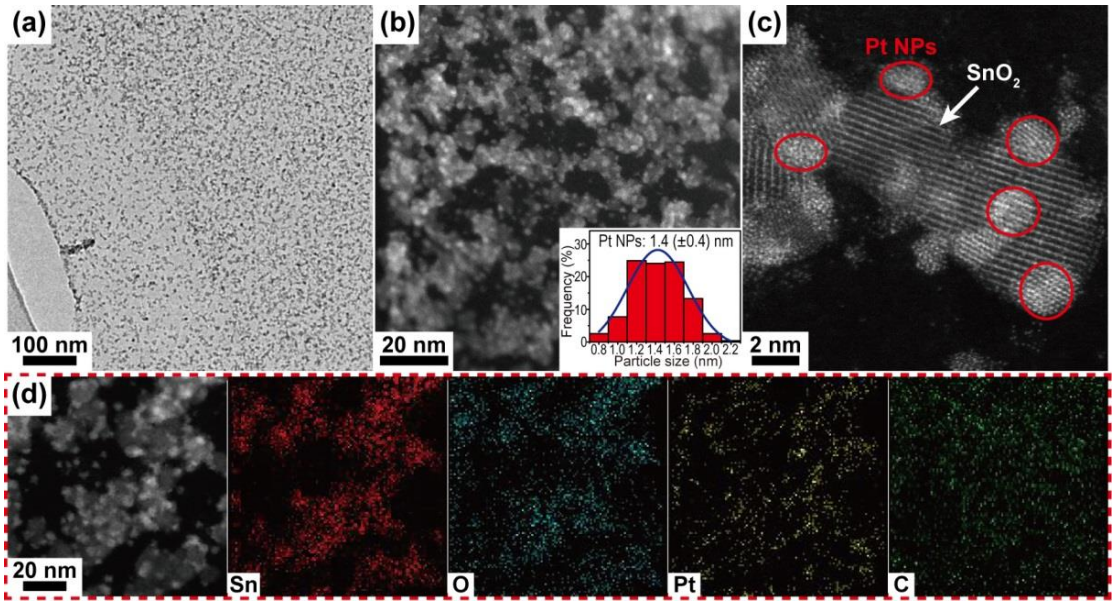

Figure 1. Representative (a) TEM, (b, c) HAADF-STEM images, and (d) EDS mapping of the prepared $Pt_{0.89}/SnO_2$/rGO NCs; (b, inset) particle size distribution histogram of Pt NPs.

The morphology of as-synthesized $Pt_{0.89}/SnO_2$/rGO NCs was characterized by TEM and HAADF-STEM. As seen from the low-magnification TEM image (Figure 1a), large quantities of small-sized NPs were uniformly dispersed on the surface of rGO

sheets. Figures 1b and c display the representative HAADF-STEM images, where ultrafine Pt NPs with an average size of 1.4 (± 0.4) nm (inset of Figure 1b) were homogeneously dispersed on the surface of SnO_2 NPs without noticeable agglomeration. The EDS mapping (Figure 1d) of as-prepared ternary hybrid clearly demonstrated the uniform distribution of all the elements including Sn, O, Pt, and C. In addition, it was also noteworthy that the Pt NPs were still firmly and uniformly anchored on the surface of SnO_2 support even after a long period of strong sonication, indicating strong interactions between Pt and SnO_2 NPs. Therefore, the rGO sheets play an important role in preventing the aggregation of Pt or SnO_2 NPs. Conversely, the highly dispersed small NPs anchored on the surface of rGO sheets can indeed act as "spacers" to prevent the overlapping of rGO sheets.

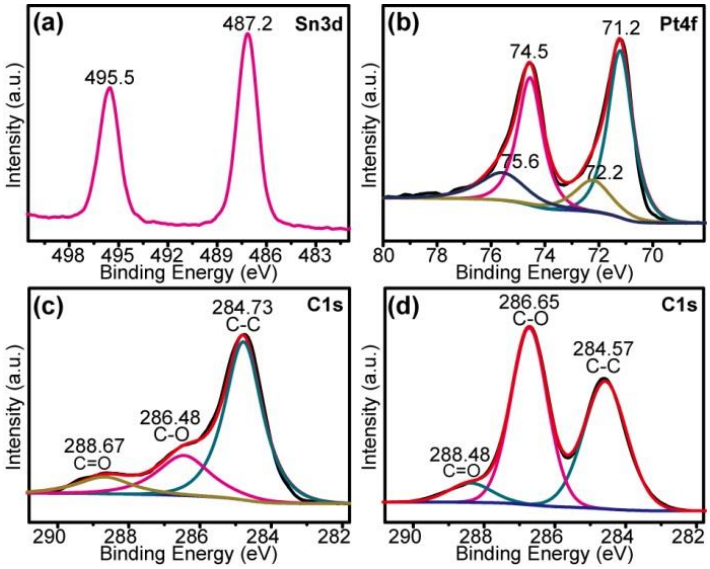

Figure 2. High-resolution XPS spectra obtained from the as-prepared $Pt_{0.89}/SnO_2$/rGO NCs: (a) Sn 3*d*, (b) Pt 4*f*, and (c) C 1*s*; (d) high-resolution C 1*s* XPS spectra of GO.

Furthermore, XPS was employed to analyze the chemical states of elements in $Pt_{0.89}/SnO_2$/rGO NCs. As shown in Figure 2a, the binding energies at 487.2 and 495.5

eV indicate that the chemical state of the element Sn in the prepared catalysts is Sn^{4+} [29]. In the Pt 4*f* XPS spectra (Figure 2b), the peaks at 71.2 eV and 74.5 eV are assigned to Pt (0), whereas the signals at 72.2 and 75.6 eV are attributed to Pt in +2 state [15]. Figure 2c displays the high-resolution C 1*s* XPS spectra, which can be divided into three peaks that correspond to carbon atoms in different oxygen-containing functional groups. The peak located at a binding energy of 284.73 eV is assigned to the C–C bond. Two other peaks located at binding energies of 286.48 and 288.67 eV respectively correspond to the C–O and C=O bonds, which show much weaker intensity compared with the peak of the C–C bond. By comparing the high-resolution C 1*s* XPS spectra from GO (Figure 2d), the peak intensity of oxygen-containing functional groups dramatically decreased, revealing that GO has been reduced to rGO [30]. Therefore, these results demonstrate that Pt/SnO_2/rGO NCs have been successfully synthesized by photo-assisted *in situ* reduction process.

As shown in Figure 3, the effects of the used H_2PtCl_6 concentration on the morphology of the catalysts were also examined. No matter how the concentration of H_2PtCl_6 changed, the ultrafine Pt NPs can be successfully assembled and closely adhered on the surface of SnO_2 supports without extensive aggregation. Also, the Pt cover density and the size of Pt NPs both increased with increasing Pt loading amount. More than 200 Pt NPs were randomly selected to determine the size distribution histograms of Pt NPs in the catalysts. The Pt NPs in the $Pt_{0.77}$/SnO_2/rGO catalysts (inset of Figure 3b) have an average size of 1.2 ($\pm$0.4) nm, whereas the size of Pt NPs in the $Pt_{1.21}$/SnO_2/rGO catalysts (inset of Figure 3e) was about 1.7 (±0.5) nm.

Figures S2a and S2b respectively show the EDS mapping of the prepared $Pt_{0.77}/SnO_2/rGO$ and $Pt_{1.21}/SnO_2/rGO$ catalysts. These two catalysts both consisted of four elements (including Sn, O, Pt, and C) and all elements were uniformly dispersed in the catalysts, thereby indicating the uniform dispersion of Pt and SnO_2 NPs on the rGO sheets. Totally, using the photo-excited electrons as reducing agents, a series of $Pt/SnO_2/rGO$ catalysts with different mass ratios of Pt and SnO_2 can be obtained by adjusting the concentration of H_2PtCl_6 in the feedstock.

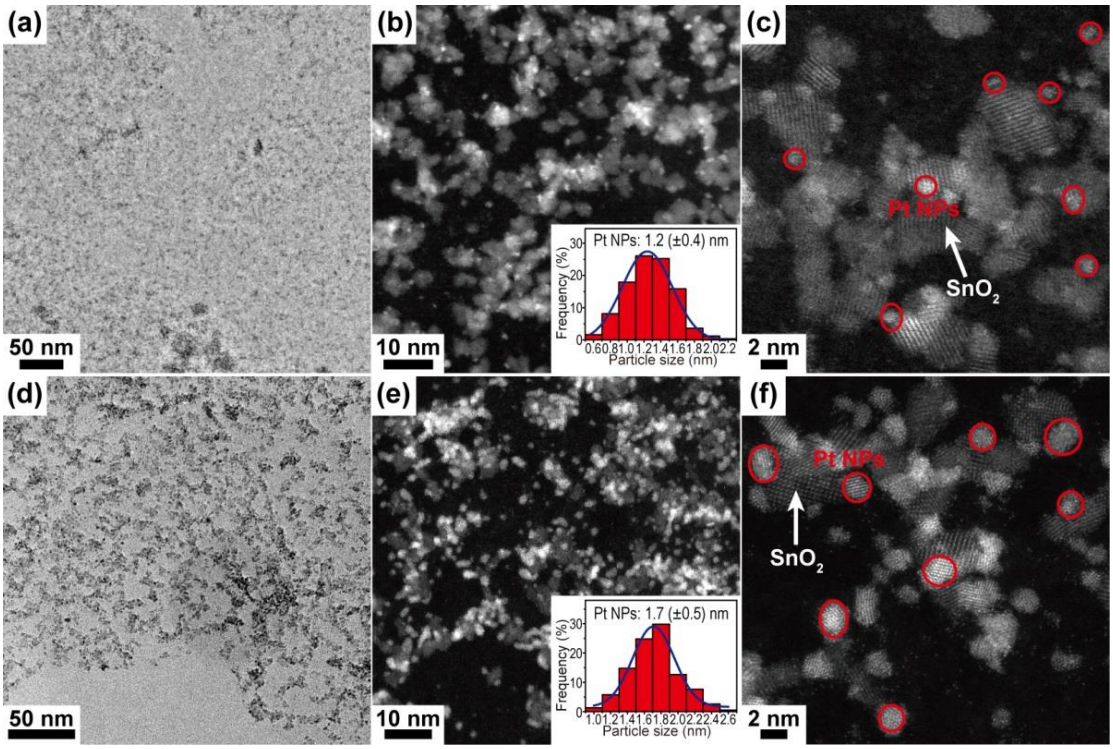

Figure 3. (a) TEM, (b, c) HAADF-STEM images of $Pt_{0.77}/SnO_2/rGO$ NCs; (d) TEM, (e, f) HAADF-STEM images of $Pt_{1.21}/SnO_2/rGO$ NCs; (b and e inset) particle size distribution histogram of Pt NPs.

3.3 Electrochemical properties of the prepared catalysts

To evaluate the potential application of as-prepared $Pt/SnO_2/rGO$ NCs, we have investigated their electrochemical properties for methanol oxidation in acidic media.

For comparison, under the same test conditions, the electrochemical measurements were also carried out with the prepared Pt/rGO catalysts, in which multiple numbers of Pt NPs with an average size of about 3.5 (±1.2) nm were attached on the surface of rGO sheets, as shown in Figure S3.

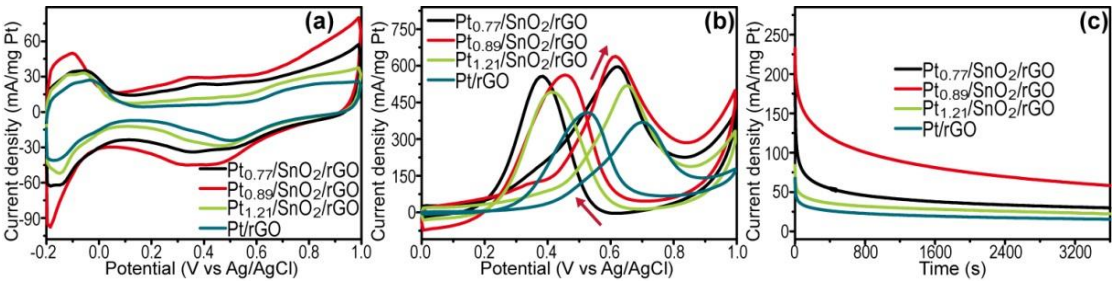

Figure 4. CV curves of GC electrodes modified with prepared catalysts measured at a scan rate of 50 mV s^{-1} in (a) 0.5 M N_2-saturated H_2SO_4 and (b) 0.5 M H_2SO_4 + 0.5 M CH_3OH; CA curves of prepared catalysts measured at in 0.5 M H_2SO_4 + 0.5 M CH_3OH at a constant potential of 0.615 V.

Table 1 Electrocatalytic properties of different catalysts

Catalyst	ECSA (cm^2/mg Pt)	Mass activity (mA/mg Pt)	Forward peak potential (V)	I_f/I_b
$Pt_{0.77}/SnO_2/rGO$	759.8	597.5	0.622	1.08
$Pt_{0.89}/SnO_2/rGO$	805.6	638.3	0.615	1.14
$Pt_{1.21}/SnO_2/rGO$	649.2	518.7	0.652	1.06
Pt/rGO	562.0	368.6	0.699	0.90

ECSA, which is proportional to the true surface area of Pt catalysts, is an important factor in determining the catalytic activity of Pt catalysts. To investigate the ECSA of the prepared catalysts, CVs were performed from −0.2 to 1 V at a scan rate of 50 mV s^{-1} in 0.5 M N_2-saturated H_2SO_4 aqueous solution, as shown in Figure 4a. Typical

hydrogen adsorption and desorption were observed between −0.2 V and 0.12 V (*vs.* Ag/AgCl). The ECSA values of the catalysts were calculated from the hydrogen adsorption area according to the following equation [31, 32]:

$$ECSA = Q_H / (0.21 \times [Pt]) \quad (4)$$

Where Q_H (in mC cm^{-2}) is the amount of charge exchanged during the electro-desorption of hydrogen atoms on Pt, 0.21 (in mC cm^{-2}) is assumed as the monolayer charge (calculated from the surface density of 1.3×10^{15} atom cm^{-2}), and [Pt] (in mg cm^{-2}) is the loading amount of Pt on the working electrode. As shown in Table 1, the $Pt_{0.77}/SnO_2/rGO$, $Pt_{0.89}/SnO_2/rGO$, and $Pt_{1.21}/SnO_2/rGO$ catalysts showed the ECSA values of 759.8, 805.6, and 649.2 cm^2 mg^{-1}, respectively, which were all higher than the Pt/rGO catalysts (562.0 cm^2 mg^{-1}). The relative larger ECSA values of the $Pt/SnO_2/rGO$ catalysts should be due to the uniform dispersion of ultrafine Pt NPs on the surface of SnO_2 supports, which was in good agreement with the observed morphology. Because of the relatively higher ECSA values, the obtained three $Pt/SnO_2/rGO$ catalysts can afford more active sites for electrochemical reaction, thereby providing the potential for better catalytic activity toward methanol oxidation.

The mass activity of Pt-based catalysts, which was normalized based on the mass of the Pt loading, was commonly adopted to compare their catalytic activities for methanol oxidation. Figure 4b shows the typical CVs of the prepared catalysts measured in a 0.5 M H_2SO_4 solution containing 0.5 M CH_3OH at a scan rate of 50 mV s^{-1}. All curves consisted of two well-defined peaks at forward and backward scans. The peak at the forward scan was assigned to the oxidation of methanol

molecules, whereas the one at the backward scan might be attributed to the oxidation of the incomplete oxidized carbonaceous species during the forward scan. The maximum current densities and the corresponding potentials were determined based on Figure 4b and the results were shown in Table 1. The current densities of the obtained four catalysts followed this order: $Pt_{0.89}/SnO_2/rGO$ > $Pt_{0.77}/SnO_2/rGO$ > $Pt_{1.21}/SnO_2/rGO$ > Pt/rGO. The $Pt_{0.89}/SnO_2/rGO$ catalysts displayed the highest current density of 638.3 mA mg^{-1}, which was about 1.73 times that of the Pt/rGO catalysts (368.6 mA mg^{-1}). Another important index, the ratio of peak current densities for the forward (I_f) and backward (I_b) scans was often used to evaluate the poisoning tolerance of the catalysts [33, 34]. A higher I_f/I_b value indicates higher tolerance to intermediate carbon species, which means that methanol can be oxidized into carbon dioxide much more efficiently with little accumulation of carbonaceous residues on the catalyst surfaces. According to the calculation based on Figure 4b, the I_f/I_b values for the $Pt/SnO_2/rGO$ catalysts were all higher than that of the Pt/rGO catalysts. In addition, the methanol oxidation peak potential was 0.615 V for the $Pt_{0.89}/SnO_2/rGO$ catalysts in comparison with an oxidation potential of 0.699 V for the Pt/rGO catalysts, which was a negative shift of 0.084 V. Thus, the addition of SnO_2 not only made the oxygen-reduction reaction easier, but also improved the tolerance toward CO poisoning of the Pt catalysts. To further describe the electrocatalytic performances of the prepared $Pt/SnO_2/rGO$ catalysts, we also compared their specific activities with those of the Pt/rGO catalysts, as shown in Figure S4. Results reveal that the specific activities of three $Pt/SnO_2/rGO$ catalysts are all higher than those of the Pt/rGO

catalysts. All of these results provide clear evidences for the superior electrocatalytic activities of the prepared Pt/SnO_2/rGO catalysts for methanol oxidation.

The stabilities of the prepared catalysts were evaluated by the CA curves at a constant potential of 0.615V in a 0.5 M H_2SO_4 solution containing 0.5 M CH_3OH for 3600 s. As shown in Figure 4c, it revealed an initial rapid current decay for all catalysts because of the formation of intermediate CO-like species during the methanol oxidation reaction [17]. Compared with the Pt/rGO catalysts, all Pt/SnO_2/rGO catalysts exhibited significantly higher initial current densities and maintained higher current densities during the entire test range, indicating more excellent catalytic activity and stability. These results are well consistent with the CV results shown in Figure 4b.

To further demonstrate the long-term stability behavior of the catalysts, continued CVs between 0 and 1 V were conducted at a scan rate of 50 mV s^{-1} for 1200 cycles. The CVs at different cycle numbers for the prepared catalysts were presented in Figures 5a–d, whereas Figures 5e and 5f respectively show the mass activities and normalized peak current densities, which were both obtained basing on the long-term tests. Clearly, all peak current densities decreased gradually with continued cycles, which may be attributed to the accumulation of intermediate species on the catalyst surface and the aggregation of Pt catalysts (see Figure S5) during the long-term CV tests. As seen from Figure 5e, the current densities for all Pt/SnO_2/rGO catalysts were higher than that of the Pt/rGO catalysts during the entire testing time. These results further proved that the Pt/SnO_2/rGO catalysts possess higher catalytic activities

toward methanol oxidation. As shown in Figure 5f, the remaining peak current density for the $Pt_{0.89}/SnO_2/rGO$ catalysts was calculated as 72.4% in relative to the initial value after 1200 cycles, which was higher than that observed from the Pt/rGO catalysts (54.5%). Moreover, the $Pt_{0.77}/SnO_2/rGO$ and $Pt_{1.21}/SnO_2/rGO$ catalysts respectively displayed the remaining forward peak current densities of 68.7% and 69.4%, both of which were also higher than that of the Pt/rGO catalysts. Therefore, these results evidently demonstrated that all $Pt/SnO_2/rGO$ catalysts possess excellent long-term stability for methanol oxidation.

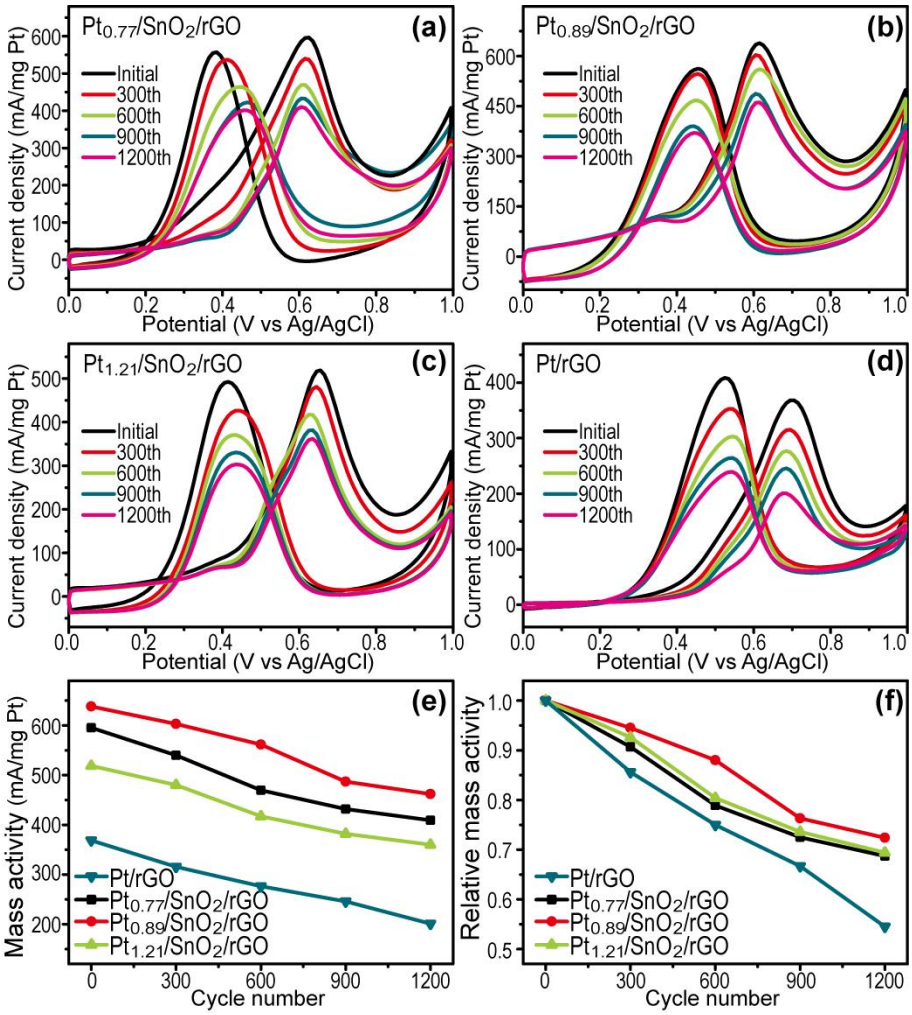

Figure 5. CVs at different cycle numbers in 0.5 M H_2SO_4 solution containing 0.5 M CH_3OH at a scan rate of 50 mV s^{-1} for (a) $Pt_{0.77}/SnO_2/rGO$, (b) $Pt_{0.89}/SnO_2/rGO$, (c) $Pt_{1.21}/SnO_2/rGO$, and (d)

Pt/rGO catalysts; (e) Mass activities and (f) the normalized peak current densities at different cycle numbers for the prepared catalysts.

The good performance of the as-prepared Pt/SnO_2/rGO catalysts toward methanol oxidation should be reasonably understood by considering the following reasons. First, the catalyst supports with large surface area can effectively prevent the Pt NPs from coalescing, thereby leading to the formation of highly dispersed, high-density, and ultrafine Pt NPs. These well-dispersed and ultrafine Pt NPs are endowed with more electrochemically active sites, active facets, and an active surface area. Also, the excellent stability of SnO_2 and graphene can retain the structural integrity of the catalysts under harsh electrochemical test conditions. The excellent conductivity of graphene could cause rapid transport of electron or charge carriers. Importantly, the synergetic effect between Pt and SnO_2 also play an important role in greatly promoting the further oxidation of CO-like species during the process of methanol oxidation, thereby leading to high stability with apparent anti-poisoning tolerance of the catalysts. During the process of methanol oxidation, methanol molecules are first absorbed on the Pt surface and subsequently disassembled as intermediate Pt-$(CO)_{ads}$. This process was described by the following equation:

$$Pt + CH_3OH \rightarrow Pt\text{-}(CO)_{ads} + H^+ + e^- \quad (5)$$

The generated CO-like species could be absorbed on the surface of Pt and take over the active sites of Pt catalysts, resulting in a rapid decrease of catalytic activity. With the addition of SnO_2, it is proposed that the oxygen-containing species (such as OH)

should be more easily formed on its surface, which are beneficial to the oxidation of CO-like species on the neighboring poisoned Pt sites and release the Pt active sites for further methanol oxidation. The possible reaction mechanism could be described as follows [14, 35]:

$$SnO_2 + H_2O \rightarrow SnO_2\text{-}OH_{ads} + H^+ + e^- \quad (6)$$

$$Pt\text{-}CO_{ads} + SnO_2\text{-}OH_{ads} \rightarrow Pt + SnO_2 + CO_2 + H^+ + e^- \quad (7)$$

Apparently, the electro-oxidation of CO-like species can be promoted only when the Pt NPs are in contact with SnO_2. In the present study, benefiting from the specific photo-assisted *in situ* reduction method, the reduced Pt NPs were strongly anchored on the surface of SnO_2, thereby resulting in better tolerance ability toward CO than the Pt/rGO catalysts.

Conclusion

We have successfully designed and prepared novel Pt/SnO_2/rGO ternary hybrid electrocatalysts by uniformly anchoring ultrafine Pt NPs onto SnO_2 in contact with rGO substrate. As anode catalysts toward methanol oxidation, these ternary hybrids displayed significantly reduced over-potential, greatly enhanced catalytic activity, and notably improved long time endurance compared with the conventional Pt catalysts supported on rGO sheets. This excellent performance was attributed to the ultrafine size of the Pt NPs and unique structure of the catalysts. The strong interaction between Pt and SnO_2 not only gives rise to a possible synergetic effect, but also greatly stabilizes the Pt catalysts. In addition, the effect of the amount of loaded Pt in

the hybrid catalysts has been systematically investigated. The results of which suggest that the component of many Pt-based catalysts could be optimized. Thus, the present work provides new clues for the design and preparation of hybrid materials in DMFCs or other energy conversion/storage applications.

Acknowledgments

This work was financial supported by the National Basic Research Program of China (2014CB931704), the National Natural Science Foundation of China (NSFC, No. 51371166, 11504375, 11304315).

Appendix A. Supplementary materials

Supplementary data associated with this article can be found in the online version at http://dx.doi.org/10.1016/j.nanoen.2016.XX.XXX.

References

[1] J. Xie, Q.H. Zhang, L. Gu, S. Xu, P. Wang, J.G. Liu, Y. Ding, Y.F. Yao, C.W. Nan, M. Zhao, Y. You, Z.G. Zou, Nano Energy 21 (2016) 247-257.

[2] R.F. Service, Science 296 (2002) 1222-1224.

[3] L.G. Feng, K. Li, J.F. Chang, C.P. Liu, W. Xing, Nano Energy 15 (2015) 462-469.

[4] A.C. Chen, P. Holt-Hindle, Chem. Rev. 110 (2010) 3767-3804.

[5] H.J. Huang, X. Wang, J. Mater. Chem. A 2 (2014) 6266-6291.

[6] W.J. Huang, H.T. Wang, J.G. Zhou, J. Wang, P.N. Duchesne, D. Muir, P. Zhang, N. Han, F.P. Zhao, M. Zeng, J. Zhong, C.H. Jin, Y.G. Li, S.T. Lee, H.J. Dai, Nat.

Commun. 6 (2015) 1-8.

[7] Y.Q. Huang, Y.J. Liu, Z.H. Yang, J.L. Jia, X. Li, Y. Luo, Y.P. Fang, J. Power Sources 246 (2014) 868-875.

[8] L. Zhao, Z.B. Wang, J.L. Li, J.J. Zhang, X.L. Sui, L.M. Zhang, J. Mater. Chem. A 3 (2015) 5313-5320.

[9] S.L. Wu, J. Liu, Z.F. Tian, Y.Y. Cai, Y.X. Ye, Q.L. Yuan, C.H. Liang, ACS Appl. Mater. Interfaces 7 (2015) 22935-22940.

[10] F.H. Li, Y.Q. Guo, Y. Liu, J. Yan, W. Wang, J.P. Gao, Carbon 67 (2014) 617-626.

[11] Z.F. Li, L. Xin, F. Yang, Y.D. Liu, Y.Z. Liu, H.Y. Zhang, L. Stanciu, J. Xie, Nano Energy 16 (2015) 281-292.

[12] J.J. Shao, Z.J. Li, C. Zhang, L.F. Zhang, Q.H. Yang, J. Mater. Chem. A 2 (2014) 1940-1946.

[13] C.Y. Zhai, M.S. Zhu, D. Bin, H.W. Wang, Y.K. Du, C.Y. Wang, P. Yang, ACS Appl. Mater. Interfaces 6 (2014) 17753-17761.

[14] F. Han, X.M. Wang, J. Lian, Y.Z. Wang, Carbon 50 (2012) 5498-5504.

[15] T.H.T. Vu, T.T.T. Tran, H.N.T. Le, L.T. Tran, P.H.T. Nguyen, H.T. Nguyen, N.Q. Bui. Electrochim. Acta 161 (2015) 335-342.

[16] C. Feng, T. Takeuchi, M.A. Abdelkareem, T. Tsujiguchi, N. Nakagawa, J. Power Sources 242 (2013) 57-64.

[17] B.Y. Xia, B. Wang, H.B. Wu, Z.L. Liu, X. Wang, X.W. Lou, J. Mater. Chem. 22 (2012) 16499-16505.

[18] X. Yu, L. Kuai, B.Y. Geng, Nanoscale 4 (2012) 5738-5743.

[19] L.T. Ye, Z.S. Li, X.F. Zhang, F.L. Lei, S. Lin, J. Mater. Chem. A 2 (2014) 21010-21019.

[20] X. Wang, X.Y. Li, D.P. Liu, S.Y. Song, H.J. Zhang, Chem. Commun. 48 (2012) 2885-2887.

[21] W.S. Hummers Jr, R.E. Offeman, J. Am. Chem. Soc. 80 (1958) 1339.

[22] Y.X. Xu, H. Bai, G.W. Lu, C. Li, G.Q. Shi, J. Am. Chem. Soc. 130 (2008) 5856-5857.

[23] Y.X. Ye, P.P. Wang, E.M. Dai, J. Liu, Z.F. Tian, C.H. Liang, G.S. Shao, Phys. Chem. Chem. Phys. 16 (2014) 8801-8807.

[24] S.H. Sun, F. Jaouen, J.P. Dodelet, Adv. Mater. 20 (2008) 3900-3904.

[25] R.Y. Wang, D.C. Higgins, M.A. Hoque, D.U. Lee, F. Hassan, Z.W. Chen, Scientific Reports 3 (2013) 1-7.

[26] Z.F. Tian, C.H. Liang, J. Liu, H.M. Zhang, L.D. Zhang, J. Mater. Chem. 21 (2011) 18242-18247.

[27] Z.F. Tian, C.H. Liang, J. Liu, H.M. Zhang, L.D. Zhang, J. Mater. Chem. 22 (2012) 17210-17214.

[28] J. Liu, Y.Y. Cai, Z.F. Tian, G.S. Ruan, Y.X. Ye, C.H. Liang, G.S. Shao, Nano Energy 9 (2014) 282-290.

[29] H.J. Wang, F.Q. Sun, Y. Zhang, L.S. Li, H.Y. Chen, Q.S. Wu, J.C. Yu, J. Mater. Chem. 20 (2010) 5641-5645.

[30] Y.M. Sun, X.L. Hu, W. Luo, Y.H. Huang, ACS Nano 5 (2011) 7100-7107.

[31] Z. Qiu, H. Huang, J. Du, T. Feng, W.K. Zhang, Y.P. Gan, X.Y. Tao, J. Phys. Chem. C 117 (2013) 13770-13775.

[32] S. Anandan, A. Manivel, M. Ashokkumar, Fuel Cells 6 (2012) 956-962.

[33] L.X. Ding, A.L. Wang, G.R. Li, Z.Q. Liu, W.X. Zhao, C.Y. Su, Y.X. Tong, J. Am. Chem. Soc. 134 (2012) 5730-5733.

[34] Y.F. Hao, Y.Y. Yang, L.J. Hong, J.H. Yuan, L. Niu, Y.H. Gui, ACS Appl. Mater. Interfaces 6 (2014) 21986-21994.

[35] F. Ye, J.J. Li, T.T. Wang, Y. Liu, H.J. Wei, J.L. Li, X.D. Wang, J. Phys. Chem. C 112 (2008) 12894-12898.